6 Search for the rare decay $\mu^+ \to e^+e^-e^+$

R. Gredig, P. Robmann, and U. Straumann

in collaboration with University of Geneva, PSI Villigen, ETH Zürich, and University of Heidelberg

(Mu3e Collaboration)

In the standard model lepton flavour is conserved at tree level. The observation of neutrino oscillations by experiments such as SuperKamiokande [1], SNO [2], and KamLAND [3] is, however, a direct proof of lepton flavour violation (LFV). Charged LFV (CLFV) would lead to $\mu \to e$ and $\tau \to \mu$ transitions without neutrinos in the final state. In the standard model CLFV can only be induced by neutrino mixing (see Fig. 6.1 for the decay of interest here) but such processes are highly suppressed by the tiny neutrino masses. The resulting branching ratios are below 10^{-50}, way beyond the experimental sensitivity. The observation of CLFV would therefore directly signal physics beyond the standard model. Two examples are shown in Fig. 6.1 as well.

Muon number violation has already been investigated in different channels (see Tab. 6.1). When these processes would be observed their relative strengths would guide the attempts to identify the underlying mechanism.

A new $\mu^+ \to e^+e^-e^+$ search has been proposed at the Paul Scherrer Institute aiming at a hitherto un-reached sensitivity down to $B < 10^{-16}$ [8], four orders of magnitude more sensitive than reached by its 25 years old predecessor SINDRUM.

TAB. 6.1 –
Experimental upper limits on the branching ratios B of LFV muon decays

Decay channel	Experiment	B upper limit	Ref.
$\mu \to e\gamma$	MEGA	1.2×10^{-11}	[4]
	MEG	2.4×10^{-12}	[5]
$\mu \to eee$	SINDRUM	1.0×10^{-12}	[6]
$\mu^-\mathrm{Au} \to e^-\mathrm{Au}$	SINDRUM II	7×10^{-13}	[7]

[1] Y. Fukuda *et al.* (Super-Kamiokande Collaboration), Phys. Rev. Lett. 81 (1998) 1562.

[2] Q.R. Ahmad *et al.* (SNO Collaboration), Phys. Rev. Lett. 87 (2001) 071301.

[3] K. Eguchi *et al.* (KamLAND Collaboration), Phys. Rev. Lett. 90 (2003) 021802.

[4] M. L. Brooks *et al.* (MEGA Collaboration), Phys. Rev. Lett. 83 (1999) 1521.

[5] J. Adam *et al.* (MEG Collaboration), Phys. Rev. Lett. 107 (2011) 171801.

[6] U. Bellgardt *et al.* (SINDRUM Collaboration), Nucl. Phys. B299 (1988) 1.

[7] W. Bertl *et al.* (SINDRUM II Collaboration), Eur. Phys. J. C47 (2006) 337.

[8] A. Blondel *et al.* (Mu3e Collaboration), *Research Proposal for an Experiment to Search for the Decay $\mu \to eee$*, Research proposal submitted to the PSI Committee for Particle Physics at the Ring Cyclotron (2013), ArXiv 1301.6113.

6.1 Experimental Requirements

The $\mu^+ \to e^+e^-e^+$ decay signal shows three decay particles with a momentum vanishing sum

$$|\vec{p}_{\mathrm{tot}}| = |\sum_i p_i| = 0\ \mathrm{MeV}/c$$

with the total energy equal to the muon mass. The most severe backgrounds are the internal conversion process $\mu^+ \to e^+e^-e^+\nu_e\overline{\nu_\mu}$ and accidental $e^+e^+e^-$ combi-

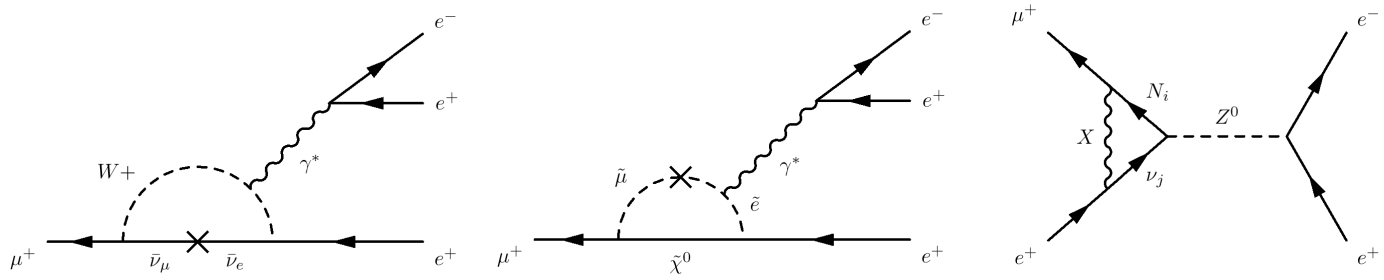

FIG. 6.1 – Possible $\mu^+ \to e^+e^-e^+$ mechanisms. From the left: neutrino mixing allowed within the standard model, a supersymmetric contribution, and a penguin diagram in the little Higgs model.

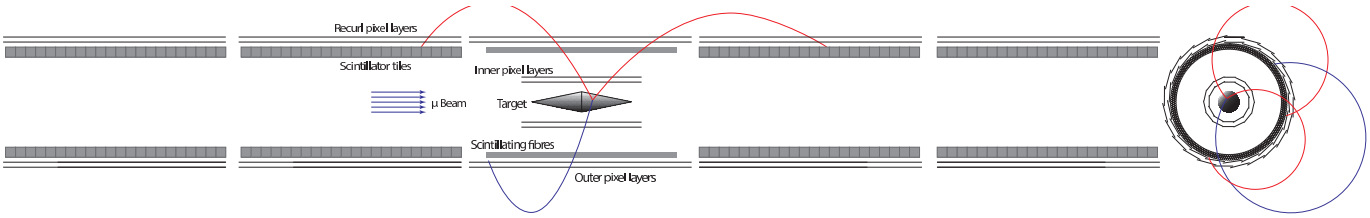

FIG. 6.2 – zr and xy views of the proposed detector.

nations. The suppression of this random background requires high time and vertex resolutions (below $\simeq$100 ps and $\simeq$100 μm, respectively). To reach the proposed high sensitivity within a few years the muon stopping rate must be at least $2\times10^9 s^{-1}$.

6.2 Proposed Detector

The proposed setup is shown in Fig. 6.2. A cylindrical detector is situated inside a 1 Tesla solenoidal magnetic field of 1 m diameter and 2.5 m length. In the centre there is a hollow aluminium double cone target with a length of 10 cm and 2 cm diameter. The muons enter along the symmetry axis. In this configuration the muons are distributed over a large area which is another measure to suppress accidental coincidences by a vertex constraint.

The detector is divided in five sub-stations along the beam-axis with a length of 36 cm each. All stations have an outer tracker built with three layers of 250 μm scintillating plastic fibres with an inner radius of 6.0 cm and two layers of silicon pixels at 7.6 cm and 8.9 cm. The central sub-detector has an additional 12 cm long inner tracker with silicon pixels at radii 1.9 cm and 2.9 cm (Fig. 6.3). This design concept is highly modular allowing a staged approach:

- Phase Ia
  This stage only uses the Si layers of the central sub-station capable of handling the muon rate of $2 \times 10^7 s^{-1}$ provided by the πE5 beam line at the PSI.

- Phase Ib
  The detector will have the first pair of re-curl stations with the corresponding scintillating tile detectors and the fibre detectors in the centre module. The improved timing resolution will allow to run at the highest πE5 rate of about $1 \times 10^8 s^{-1}$.

- Phase II
  In this final phase all five sub-stations will be available and a new beam line (HiMB) will provide the $2 \times 10^9 s^{-1}$ muon rate required for the ultimate sensitivity

6.3 Scintillating Fibres

The Mu3e group at UZH develops the scintillating fibre tracker in close collaboration with the University of Geneva and the ETH Zürich. The light of the fibres will be read out with silicon photomultipliers (SiPM). The advantages of such light detectors are the small size and that they can be operated in a high magnetic field.

In a first step a simulation tool-kit using GEANT4 has been developed to study the optical response of the fibres. The simulation has two sequential modes of operation which minimises the required computer time:

- For a detailed analysis of a specific fibre geometry it is used standalone. The generation, propagation and absorption of the photons in the fibre are simulated and the fibre response as a function of the crossing position and energy deposit is parametrized.

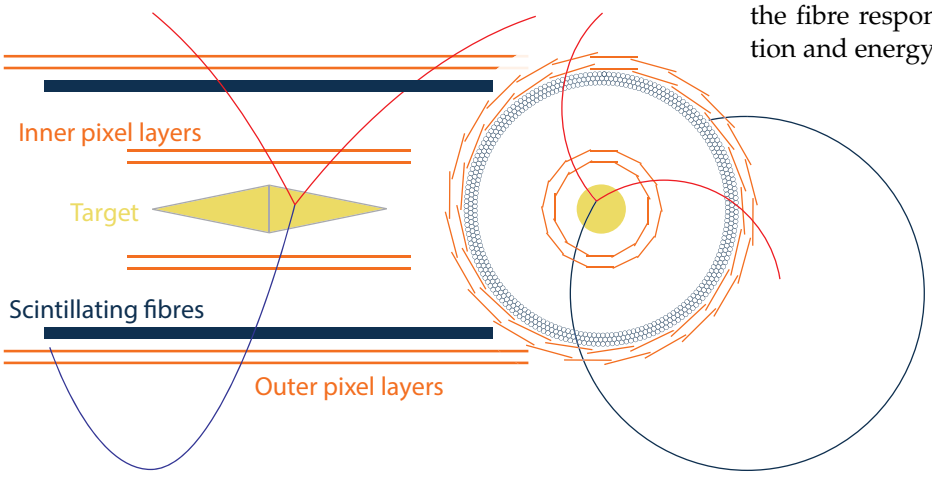

FIG. 6.3 – Expanded view of Fig. 6.2 with the scintillating fibres highlighted in blue. The fibres are not to scale.

- The simulation covering the whole detector no longer tracks the scintillation light but uses the parametrized fibre response instead.

The simulation of the light propagation allows to compare different fibre geometries, coatings and staggering schemes. Not only the spatial distribution of the photons (see Fig. 6.5) but also their time distribution has been studied. For a single fibre typically 12 photons reach one end of the fibre (see Fig. 6.6) where they will be detected with an efficiency of typically 50% with a SiPM array. The signal shape has been studied including the response of the light sensor [1] and the results indicate a time resolution of ∼400 ps.

[1] P. Eckert *et al.*, JINST 7 (2012) P08011.

6.4 Test Setup

A test setup is currently under development at the institute to verify the simulation results. The setup includes a support for the scintillating fibres, several photomultiplier tubes to measure the generated light and a radioactive source. It will also allow to analyse different fibre staggering geometries (Fig. 6.4) and to study the corresponding light yield and the optical crosstalk.

Currently the photomultiplier tubes (PMT) are being calibrated with a pulsed laser to obtain the single-photoelectron response. The PMTs are exposed to a strongly attenuated laser resulting in zero photons most of the time. The signal gating is triggered by the laser. Fig. 6.7 shows the resulting charge distribution for a Burle S83062E PMT. A narrow spike at zero originates in events with zero photoelectrons (p.e.). Broad bumps originate from events with 1, 2 or 3 p.e. where the widths result from the gains in the first dynodes as reproduced by a model of the PMT response [1].

After positioning three fibres in a row the photon yield of the central fibre will be determined by using the signals from the two other fibres as a trigger. Finally, the test setup will be completed with SiPM sensors, amplification and digitisation electronics as used later on.

[1] E. H. Bellamy *et al.*, NIM 339 (1994) 468.

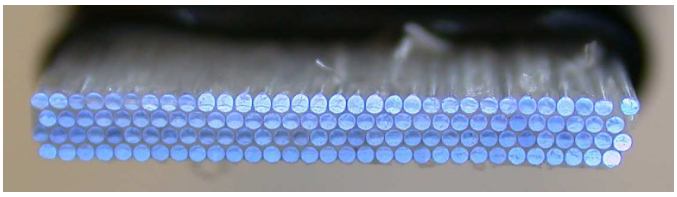

FIG. 6.4 – Ribbon of glued scintillating fibres (produced by the Geneva group).

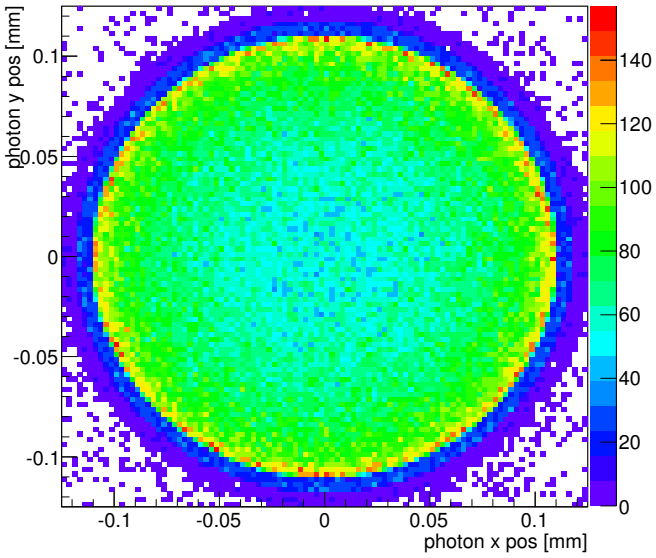

FIG. 6.5 – xy distribution of the photon at the fibre end. 30 thousand events were generated in which a 15 MeV positron is emitted towards the fibre centre.

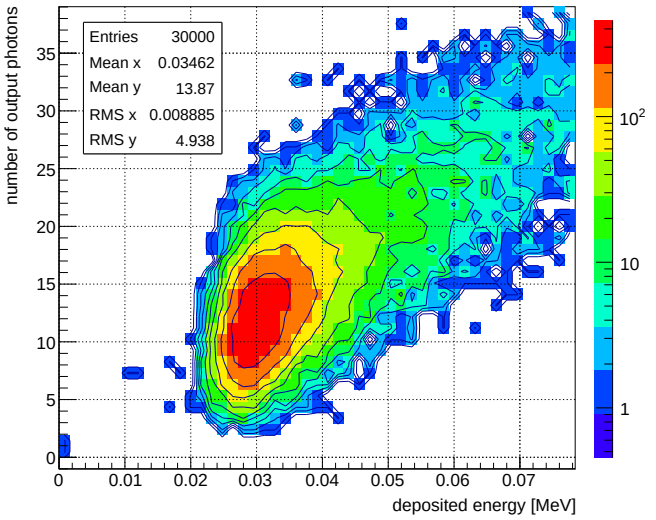

FIG. 6.6 – Photon yield at one fibre end versus energy deposit for a 15 MeV positron crossing the fibre centre.

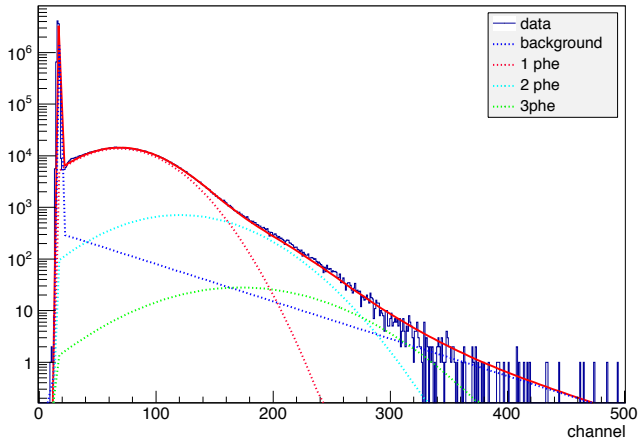

FIG. 6.7 – Charge response (arbitrary units) of a Burle S83062E PMT to 1×10^7 laser triggers. The measured data are well reproduced by a model [1].